



ARMA/USRMS 06-1069

Embedded discontinuity finite element modeling of three-dimensional strong discontinuities in rocks

Regueiro, R.A.

Department of Civil, Environmental, and Architectural Engineering, University of Colorado at Boulder, Boulder, CO 80309, U.S.A.

Copyright 2006, ARMA, American Rock Mechanics Association

This paper was prepared for presentation at Golden Rocks 2006, the 41st U.S. Symposium on Rock Mechanics (USRMS): "50 Years of Rock Mechanics - Landmarks and Future Challenges." Golden, Colorado, June 17-21, 2006.

This paper was selected for presentation by a USRMS Program Committee following review of information contained in an abstract submitted earlier by the author(s). Contents of the paper, as presented, have not been reviewed by ARMA/USRMS and are subject to correction by the author(s). The material, as presented, does not necessarily reflect any position of USRMS, ARMA, their officers, or members. Electronic reproduction, distribution, or storage of any part of this paper for commercial purposes without the written consent of ARMA is prohibited. Permission to reproduce in print is restricted to an abstract of not more than 300 words; illustrations may not be copied. The abstract must contain conspicuous acknowledgement of where and by whom the paper was presented.

ABSTRACT: Localized deformation such as shear bands, compaction bands, dilation bands, combined shear/compaction or shear/dilation bands, fractures, and joint slippage are commonly found in rocks. Thus, modeling their inception, development and propagation, and effect on stress response is important with regard to making informed engineering design decisions involving these materials. Following a GulfRocks04 paper (ARMA/NARMS 04-520) that focused on modeling bifurcation to these localized deformations, this paper focuses on modeling numerically the post-bifurcation regime, specifically strong discontinuities in rock whose bulk response is governed by a three-invariant, isotropic/kinematic hardening cap plasticity model. We develop a simple post-bifurcation constitutive model and implement it using an enhanced strain finite element method, an approach used to embed discontinuities within the coarse scale finite element response. The post-bifurcation model takes the form of a simple Mohr-Coulomb failure model along the discontinuity, but with internal variables cohesion, dilation/compaction, and friction allowed to degrade linearly or exponentially as a function of jump displacement across a discontinuity/crack. Because the dilation/compaction internal variable evolves, the enhancement function for the enhanced strain finite element formulation evolves as well. A hexahedral Embedded Discontinuity finite Element (EDE) is implemented to model three-dimensional strong discontinuities in rock. Numerical examples will demonstrate the model.

1. INTRODUCTION

Localized deformation can be triggered either by material inhomogeneities such as joint sets in rocks and/or by inhomogeneous stresses resulting from boundary conditions such as friction at end platens in a confined compression test or from the geometry of a problem (such as an underground tunnel), for instance. Localized deformation does not always lead to immediate catastrophic failure, in that a shear band or crack could be arrested, depending on the loading conditions applied to the tunnel walls, for example. Localized deformation could lead, however, to immediate catastrophic failure as a worst case, and eventual failure of the tunnel over the lifetime of the structure. Thus, modeling the inception, development and propagation of localized deformation, and its effect on stress response is important

with regard to making informed engineering design decisions. In order to make informed decisions for complex three-dimensional (3D) geometries, loading conditions, and nonlinear material behavior, numerical modeling of failure in rock is essential because analytical solutions would be unworkable. With parallel computing becoming more commonplace, and with the advent of molecular (and possibly even quantum) computing becoming a reality in our lifetimes, solving these complex 3D failure problems with numerical models is feasible. Applications of pre- and post-bifurcation constitutive models and a computational framework for modeling localized deformation in rock include assessing the long term performance of nuclear waste repositories, designing tunnel construction, oil and natural gas production, and depleted reservoirs used for subsurface seques-

tration of greenhouse gases.

Following a GulfRocks04 paper [1] that focused on modeling the bifurcation to these localized deformations, this paper focuses on modeling numerically the post-bifurcation regime, specifically strong discontinuities in rock whose bulk response is governed by a three-invariant, isotropic/kinematic hardening cap plasticity model [2, 3]. A simple post-bifurcation constitutive model is implemented using an enhanced strain finite element method, an approach used to embed discontinuities within the coarse scale finite element response. The post-bifurcation model takes the form of a simple Mohr-Coulomb failure model along the discontinuity, but with internal variables cohesion, dilation/compaction, and friction allowed to degrade linearly or exponentially as a function of jump displacement across a discontinuity/crack. Because the dilation/compaction internal variable evolves, the enhancement function for the enhanced strain finite element formulation evolves as well. A hexahedral Embedded Discontinuity finite Element (EDE) is implemented to model 3D strong discontinuities in rock.

Throughout the paper we assume small deformations and rotations. Symbolic notation is used for clearer presentation, such as the inner product of two second order tensors $(\mathbf{a} \cdot \mathbf{b})_{ik} = a_{ij}b_{jk}$, the contraction of two tensors $\mathbf{a} : \mathbf{b} = a_{ij}b_{ij}$, or the dyadic product $(\mathbf{a} \otimes \mathbf{b})_{ijkl} = a_{ij}b_{kl}$. Tensor operators are used such as the symmetric gradient $(\nabla^s \mathbf{v})_{ij} = (v_{i,j} + v_{j,i})/2$, and divergence $(\nabla \cdot \mathbf{a})_i = a_{ij,j}$. The symbol $(\dot{\bullet}) = \partial(\bullet)/\partial t$ denotes a time derivative.

2. KINEMATICS AND GOVERNING EQUATIONS FOR STRONG DISCONTINUITIES

For strong discontinuities, the velocity field contains a spatial jump in velocity $[[\mathbf{v}]]$ across \mathcal{S} as [10]

$$\mathbf{v}(\mathbf{x}, t) = \bar{\mathbf{v}}(\mathbf{x}, t) + [[\mathbf{v}(\mathbf{x}, t)]] H_S(\mathbf{x}) \quad (1)$$

where $\bar{\mathbf{v}} = \partial \bar{\mathbf{u}} / \partial t$ is the regular velocity field, and H_S is the Heaviside function along surface \mathcal{S} (cf. Fig.1). This velocity field leads to a singular strain rate $\dot{\epsilon} = \nabla^s \mathbf{v}$ at \mathcal{S} as

$$\dot{\epsilon} = \begin{cases} \dot{\epsilon}^1 = \dot{\epsilon}^0 + \text{sym}([[\mathbf{v}]] \otimes \mathbf{n}) \delta_S & \in \mathcal{S} \\ \dot{\epsilon}^0 & \in \Omega \setminus \mathcal{S} \end{cases} \quad (2)$$

where superscript 1 denotes a quantity along \mathcal{S} and superscript 0 a quantity outside \mathcal{S} , where $\dot{\epsilon}^0$ is regular

and $\dot{\epsilon}^1$ is singular. δ_S is the Dirac-delta function at the discontinuity surface \mathcal{S} , and \mathbf{n} is the unit normal to \mathcal{S} .

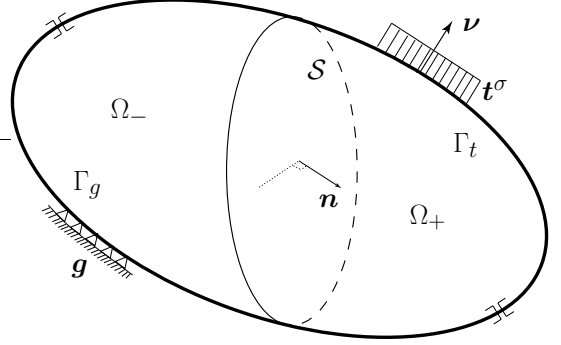


Figure 1. Body $\bar{\Omega}$ with planar strong discontinuity \mathcal{S} ($\Omega = \Omega_+ \cup \Omega_-$, $\Gamma = \Gamma_t \cup \Gamma_g \cup \mathcal{S}$, $\bar{\Omega} = \Omega \cup \Gamma$).

The local form of quasi-static, isothermal equilibrium for a body Ω with strong discontinuity is written as follows

$$\begin{aligned} \nabla \cdot \boldsymbol{\sigma} + \mathbf{b} &= \mathbf{0} & \text{in } \Omega \\ \boldsymbol{\sigma} \cdot \boldsymbol{\nu} &= \mathbf{t}^\sigma & \text{on } \Gamma_t \\ \mathbf{u} &= \mathbf{g} & \text{on } \Gamma_g \\ [[\boldsymbol{\sigma}]] \cdot \mathbf{n} &= \mathbf{0} & \text{across } \mathcal{S} \end{aligned} \quad (3)$$

where $\boldsymbol{\sigma}$ is the stress tensor, \mathbf{b} the body force vector, $\boldsymbol{\nu}$ the unit normal to Γ_t , \mathbf{t}^σ the traction on Γ_t , \mathbf{g} the prescribed displacement on Γ_g , and $[[\boldsymbol{\sigma}]]$ is the jump in stress across \mathcal{S} .

The variational form of quasi-static equilibrium can then be written as

$$\begin{aligned} \int_{\Omega} \nabla^s \boldsymbol{\eta} : \boldsymbol{\sigma} \, d\Omega &= \int_{\Omega} \boldsymbol{\eta} \cdot \mathbf{b} \, d\Omega + \int_{\Gamma_t} \boldsymbol{\eta} \cdot \mathbf{t}^\sigma \, d\Gamma \\ &+ \int_{\mathcal{S}} \boldsymbol{\eta} \cdot ([[\boldsymbol{\sigma}]]) \cdot \mathbf{n} \, d\Gamma \end{aligned} \quad (4)$$

where $\boldsymbol{\eta} = \delta \mathbf{u}$ is the weighting function (or displacement variation). The traction continuity condition $[[\boldsymbol{\sigma}]] \cdot \mathbf{n} = \mathbf{0}$ for a body with strong discontinuities will be used to determine bifurcation.

3. DETECTING BIFURCATION

The bifurcation analysis follows that conducted in [1] and will only be briefly summarized here. As reported in the literature (Sandler & Wright [4], Needleman [5], Sluys & de Borst [6]), viscous regularization in the manner of Duvaut-Lions inhibits loss of strong ellipticity for strain-softening plasticity

models, assuming the viscosity is finite. For a nearly rate insensitive model (viscosity $\eta \approx 0$), however, loss of strong ellipticity via the underlying inviscid model is possible. Bifurcation analysis of the rate insensitive (inviscid) and rate sensitive forms of the model is summarized.

3.1. Rate insensitive model and bifurcation with strong discontinuity

Assume the jump velocity is spatially constant along \mathcal{S} and is written in terms of its magnitude $\dot{\zeta}$ and direction \mathbf{m} as

$$[[\mathbf{v}(t)]] = \dot{\zeta}(t) \mathbf{m}(t) \quad (5)$$

Note that its magnitude and direction can both vary with time, mainly that since the dilation/compaction angle ψ (cf. Fig.2) can evolve during post-bifurcation, $\mathbf{m}(t)$ can change.

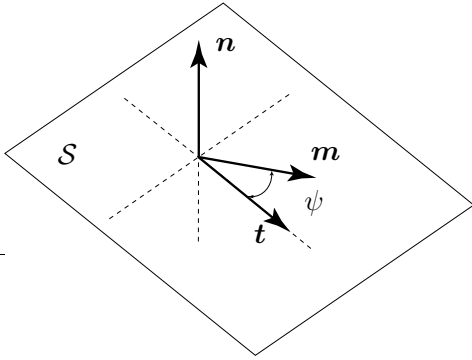


Figure 2. Band normal \mathbf{n} , tangent \mathbf{t} , and velocity jump direction \mathbf{m} with dilation/compaction angle ψ .

For continuous traction across the discontinuity surface \mathcal{S} , a condition for loss of ellipticity of the acoustic tensor $\tilde{\mathbf{A}}$ results as

$$\det \tilde{\mathbf{A}} = 0 \quad \text{for } \mathbf{m} \neq \mathbf{0} \quad (6)$$

$$\begin{aligned} \tilde{\mathbf{A}} &= \mathbf{n} \cdot \tilde{\mathbf{c}}^{ep} \cdot \mathbf{n} \\ \tilde{\mathbf{c}}^{ep} &= \mathbf{c}^e - \frac{\mathbf{c}^e : \mathbf{g} \otimes \mathbf{f} : \mathbf{c}^e}{\mathbf{f} : \mathbf{c}^e : \mathbf{g}} \\ \mathbf{f} &= \partial f / \partial \boldsymbol{\sigma} ; \quad \mathbf{g} = \partial g / \partial \boldsymbol{\sigma} \end{aligned} \quad (7)$$

where \mathbf{c}^e is the elastic modulus tensor, $\tilde{\mathbf{c}}^{ep}$ is the continuum elastic-perfectly-plastic tangent modulus tensor, f is the yield function, and g is the plastic potential function. It was shown in [1] that the same bifurcation condition results for continuous and discontinuous bifurcation [7] for the case of strong discontinuity localized kinematics.

3.2. Discrete form of rate sensitive model

Bifurcation analysis of the discrete form of a rate sensitive model allows one to analyze acoustic tensors to determine mathematical instability of the underlying constitutive model. To ensure continuous traction, we have

$$\begin{aligned} \hat{\mathbf{A}} \cdot \mathbf{m} &= \mathbf{0} \\ \hat{\mathbf{A}} &= \mathbf{n} \cdot \hat{\mathbf{c}}^{ep} \cdot \mathbf{n} \\ \hat{\mathbf{c}}^{ep} &= (1 - \exp[-\Delta t / \tau]) (\tilde{\mathbf{c}}^{ep} + (\tau / \Delta t) \mathbf{c}^e) \\ \tau \rightarrow 0 &\implies \hat{\mathbf{c}}^{ep} = \tilde{\mathbf{c}}^{ep} \\ \tau \rightarrow \infty &\implies \hat{\mathbf{c}}^{ep} = \mathbf{c}^e \end{aligned} \quad (8)$$

where Δt is the discrete time increment, and τ is the relaxation time such that $\tau \rightarrow 0$ leads to the inviscid solution and $\tau \rightarrow \infty$ to the elastic solution. As shown in [1], the same bifurcation condition for $\tau \rightarrow 0$ results for continuous and discontinuous bifurcation with strong discontinuity. For finite $\tau > 0$, $\hat{\mathbf{c}}^{ep}$ could remain positive definite, i.e. that $\det \hat{\mathbf{A}} > 0$, depending on the strain rate. The following example demonstrates the effect of τ and the strain rate on bifurcation. Using Sandia GeoModel parameters given in Table 1 for Salem Limestone [2], along with a relaxation time $\tau = 5e-4$ sec, loss of ellipticity is checked for 0.025/sec, 0.25/sec, and 2.5/sec strain rates. As shown in Fig.3, loss of ellipticity is detected for the 0.025/sec and 0.25/sec strain rates, while it is inhibited for the 2.5/sec strain rate, a result that is well documented in the literature (cf. [5]).

4. POST-BIFURCATION CONSTITUTIVE MODEL

The general form of a post-bifurcation traction-displacement constitutive model is the following:

$$\mathbf{T} = [T_n \ T_t] \quad (9)$$

$$T_n = \mathbf{n} \cdot \boldsymbol{\sigma} \cdot \mathbf{n} ; \quad T_t = \mathbf{t} \cdot \boldsymbol{\sigma} \cdot \mathbf{n}$$

$$[[\dot{\mathbf{u}}]] = \dot{\gamma}_\delta \partial G(\mathbf{T}, \mathbf{q}) / \partial \mathbf{T} \quad (10)$$

$$F(\mathbf{T}, \mathbf{q}) = 0 \quad (11)$$

$$\dot{\mathbf{q}} = \dot{\gamma}_\delta \mathbf{h}^q \quad (12)$$

where \mathbf{T} is the traction vector on \mathcal{S} , \mathbf{t} is the unit tangent vector on \mathcal{S} , $[[\dot{\mathbf{u}}]] = \dot{\zeta} \mathbf{m}$ is the rate of jump displacement or jump velocity, $\dot{\gamma}_\delta$ is an internal inelastic multiplier on \mathcal{S} , G is an inelastic potential function, F is an inelastic yield function, \mathbf{q} is a vector

| Symbol | Value |
|------------|------------------------|
| E | 22.5 GPa |
| ν | 0.25 (dimensionless) |
| A | 690 MPa |
| B | $3.9\text{e-}4$ 1/MPa |
| C | 675 MPa |
| θ | 0.0 radians |
| R | 28.0 (dimensionless) |
| κ_0 | -8.0 MPa |
| W | 0.08 (dimensionless) |
| D_1 | $1.5\text{e-}3$ 1/MPa |
| D_2 | 0.0 1/MPa ² |
| c^α | $1.0\text{e}5$ MPa |
| ψ | 1.0 (dimensionless) |
| N | 6.0 MPa |

Table 1. Sandia GeoModel Parameters for Salem Limestone.

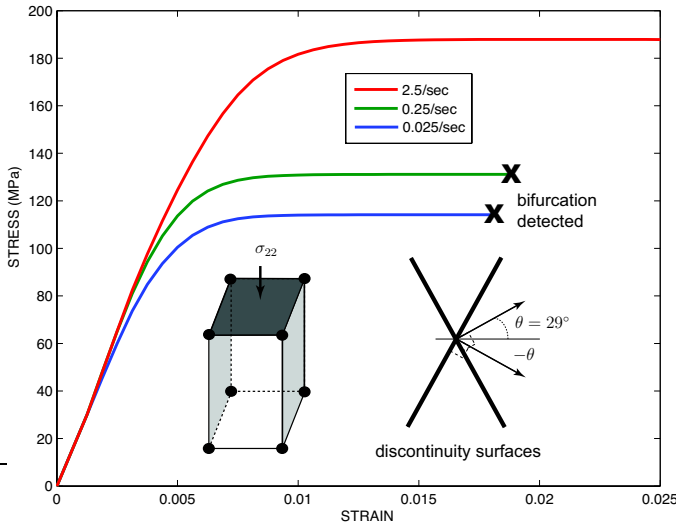


Figure 3. Plot of stress versus strain for bifurcation analysis of plane strain compression of Salem Limestone using the Sandia GeoModel. One trilinear hexahedral element 4cm wide by 8cm high by 8cm deep ($4 \times 8 \times 8$ cm) is used for the plane strain simulations.

of internal strength variables (e.g., cohesion c , friction angle ϕ , dilation/compaction angle ψ), and \mathbf{h}^q is a vector of softening functions. A Mohr-Coulomb traction-displacement model with exponential softening is summarized as

$$\begin{aligned}
 F &= |T_t| - (c - T_n^* \tan \phi) = 0 \\
 G &= |T_t| - (c - T_n^* \tan \psi) \\
 c &= c_r + (c_p - c_r) \exp(-\alpha_c \gamma_\delta)
 \end{aligned} \tag{13}$$

$$\begin{aligned}
 \gamma_\delta &= \int_0^t \dot{\gamma}_\delta dt; \quad \dot{\gamma}_\delta = \cos \psi \dot{\zeta} \\
 \phi &= \phi_r + (\phi_p - \phi_r) \exp(-\alpha_\phi \gamma_\delta) \\
 \psi &= \psi_p \exp(-\alpha_\psi \gamma_\delta)
 \end{aligned}$$

where $T_n^* = (T_n - |T_n|)/2$ is negative for compressive traction and zero in tension, and the vector of internal variables is

$$\mathbf{q} = [c \quad \phi \quad \psi]^T \tag{14}$$

Subscript $(\bullet)_r$ refers to residual value, and $(\bullet)_p$ peak value. The material parameters α_c , α_ϕ , and α_ψ control the rate of softening for each internal variable. The implementation of this model using an EDE formulation is discussed in the next section.

5. EMBEDDED DISCONTINUITY FINITE ELEMENT (EDE)

This section describes an Embedded Discontinuity finite Element (EDE) implementation using an assumed enhanced strain method [8, 10]. We will discuss a reparameterization of the displacement field and introduction of an embedded discontinuity enhancement function for a hexahedral element, the Petrov-Galerkin form for the three-field variational equations, an orthogonality condition and patch test, discrete time integration of stress and traction-displacement model, the traction-displacement relation in weak form using method of weighted residuals, how to determine yielding on \mathcal{S} , linearization for iterative solution, a linear softening model, and how to ensure continuous stress in time from pre to post-bifurcation.

5.1 Reparameterization of displacement \mathbf{u}^h by introduction of enhancement function f_S^e for EDE

Because we would like to interpolate compatible displacements at the nodes, the jump displacement may be embedded within the element, such that the discrete representation of displacement is now reparameterized as [10]

$$\begin{aligned}
 \mathbf{u}^h &= (\bar{\mathbf{u}}^h + [[\mathbf{u}^h]] f_S^e) + [[\mathbf{u}^h]] (H_{\mathcal{S}^h} - f_S^e) \\
 &= \tilde{\mathbf{u}}^h + \hat{\mathbf{u}}^h \\
 \tilde{\mathbf{u}}^h &= \bar{\mathbf{u}}^h + [[\mathbf{u}^h]] f_S^e \\
 \hat{\mathbf{u}}^h &= [[\mathbf{u}^h]] (H_{\mathcal{S}^h} - f_S^e) \\
 M_{\mathcal{S}^h} &= H_{\mathcal{S}^h} - f_S^e
 \end{aligned} \tag{15}$$

where h is the spatial discretization parameter [15], \tilde{u}^h is the compatible displacement, \hat{u}^h is the enhanced displacement, f_S^e is a smooth enhancement function within element e to ensure that \tilde{u}^h is compatible and M_{Sh} is zero at the nodes of the EDE. Figure 4 illustrates this reparameterization for a one dimensional (1D) linear finite element. The regular displacement $\bar{u}^h(x)$ interpolates linearly the incompatible displacement between nodes 1 and 2. The compatible displacement $\tilde{u}^h(x)$ interpolates linearly the compatible displacement between nodes 1 and 2 and is by definition compatible across elements. The enhancement function f_S^e is introduced to generate M_{Sh} such that when multiplied by $[[u]]$ and added to the compatible displacement $\tilde{u}^h(x)$ yields the desired displacement field $u^h(x)$ in one dimension.

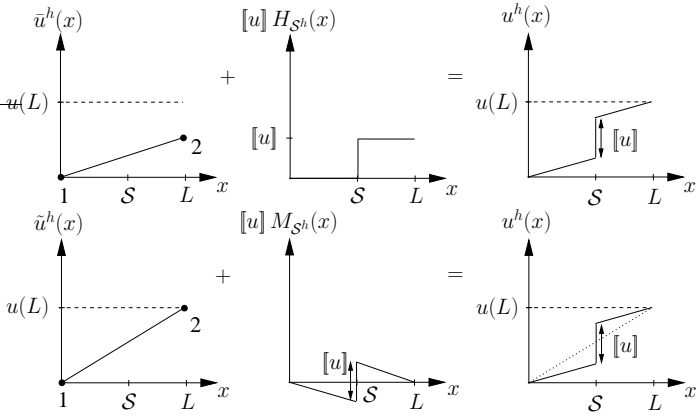


Figure 4. 1D motivation for the construction of M_{Sh} .

We will interpolate the compatible displacement using standard finite element shape functions N_a as

$$\tilde{u}^h(\boldsymbol{\xi}, t) = \sum_{a=1}^{n_{en}} N_a(\boldsymbol{\xi}) \mathbf{d}_a(t) \quad (16)$$

where $\boldsymbol{\xi}$ is the vector of natural coordinates and n_{en} is the number of element nodes.

To complete the 3D EDE formulation, the enhancement function f_S^e for a 3D element must be determined. For a linear hexahedral element, various ways in which a planar strong discontinuity can cut the element are depicted in Fig.5. The procedure for determining the active nodes, and thus the enhancement function f_S^e is shown in Fig.6, where the enhancement function is written as

$$f_S^e(\boldsymbol{\xi}) = \sum_{b=1}^{n_{active}} N_b(\boldsymbol{\xi})$$

With coordinates of a point \mathbf{x}^s on the discontinuity surface S^e for element e , and with the normal to the

surface \mathbf{n} , we can determine an active node by the following: if $\mathbf{n} \cdot (\mathbf{x}^b - \mathbf{x}^s) > 0$ then node b is active where \mathbf{x}^b is the coordinate vector of node b . This procedure should work for higher order elements as well, although the procedure has not been tested for a higher order hexahedral element.

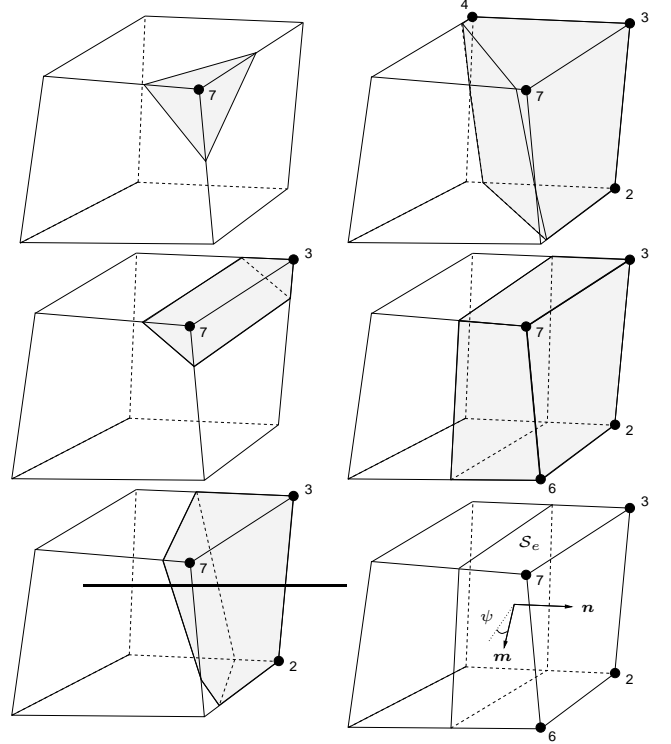


Figure 5. Embedded strong discontinuity linear hexahedral finite element.

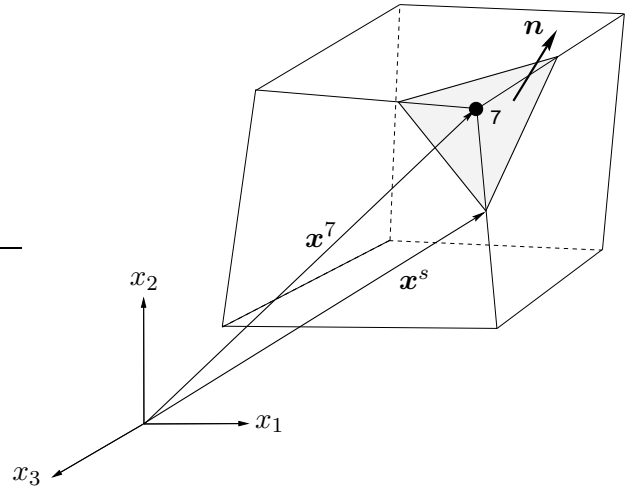


Figure 6. Determination of active nodes and embedded strong discontinuity enhancement function f_S^e .

5.2 Petrov-Galerkin variational equations

The Petrov-Galerkin variational equations are derived from the three-field variational form [8] leading to the following equations

$$\begin{aligned} \int_{\Omega^h} \nabla^s \tilde{\mathbf{w}}^h : \boldsymbol{\sigma}^h dv &= \int_{\Omega^h} \tilde{\mathbf{w}}^h \cdot \mathbf{b} dv + \int_{\Gamma_t^h} \tilde{\mathbf{w}}^h \cdot \mathbf{t}^\sigma da \\ \int_{\Omega_{\text{loc}}^h} \hat{\boldsymbol{\gamma}}^h : \boldsymbol{\sigma}^h dv &= 0 \end{aligned} \quad (17)$$

where $\tilde{\mathbf{w}}^h$ is the compatible weighting function, Ω_{loc}^h the domain in which elements have localized, and $\hat{\boldsymbol{\gamma}}^h$ the enhanced strain variation. Equation (17)₁ is the standard balance of linear momentum, and Eq.(17)₂ is known as the orthogonality condition. We will use the orthogonality condition when writing our traction-displacement model in weak form, and the patch test will need to pass in order to ensure convergence (i.e., $\mathbf{u} = \lim_{h \rightarrow 0} \mathbf{u}^h$).

From [13], we assume an enhanced strain variation that must satisfy the orthogonality condition

$$\hat{\boldsymbol{\gamma}}^h = \eta^h \left(\frac{\delta_{S^h}}{A_{S^h}} - \frac{1}{V_{\text{loc}}^h} \right) \hat{\mathbf{H}}^h \quad (18)$$

where η^h is a scalar weighting function, δ_{S^h} is the Dirac-delta function at S^h , A_{S^h} is the area of S^h , V_{loc}^h is the localized volume, and $\hat{\mathbf{H}}^h$ is an arbitrary second order tensor that will be chosen based on the choice of traction-displacement model [13]. Given Eq.(18), the orthogonality condition reads

$$\frac{1}{A_{S^h}} \int_{S^h} \eta^h \hat{\mathbf{H}}^h : \boldsymbol{\sigma}^h da - \frac{1}{V_{\text{loc}}^h} \int_{\Omega_{\text{loc}}^h} \eta^h \hat{\mathbf{H}}^h : \boldsymbol{\sigma}^h dv = 0$$

Note that $1/A_{S^h}$ and $1/V_{\text{loc}}^h$ can be placed outside the integral because for small deformations the current areas and volumes approximately equal the reference ones. For finite deformations, this would not be the case [9].

5.3 Patch test

In [16], the patch test essentially states that constant stress fields must be admissible in the solution space. This means that as the mesh is refined, the finite elements reduce in size to a point ($h \rightarrow 0$), and the finite element solution must approach the exact solution of the partial differential equation, which at a point has a constant stress value. Here, this can be

stated as $\boldsymbol{\sigma}^h = \boldsymbol{\sigma}_0$, where $\boldsymbol{\sigma}_0$ is constant, and then the orthogonality condition Eq.(17)₂ reads [8, 9]

$$\left[\int_{\Omega_{\text{loc}}^h} \hat{\boldsymbol{\gamma}}^h dv \right] : \boldsymbol{\sigma}_0 = 0 \quad (19)$$

which is satisfied if

$$\int_{\Omega_{\text{loc}}^h} \hat{\boldsymbol{\gamma}}^h dv = \mathbf{0} \quad (20)$$

which, when substituting Eq.(18) into Eq.(20), leads to

$$\frac{1}{A_{S^h}} \int_{S^h} \eta^h \hat{\mathbf{H}}^h da = \frac{1}{V_{\text{loc}}^h} \int_{\Omega_{\text{loc}}^h} \eta^h \hat{\mathbf{H}}^h dv \quad (21)$$

For constant η^h and $\hat{\mathbf{H}}^h$ within a localized element e , this condition would be satisfied trivially, and then the patch test would pass. For generality, however, we leave this condition as is because in the future we would like to consider spatially-varying ζ on S^h and in Ω_{loc}^h . For most enhanced strain implementations of embedded strong discontinuities [10, 11, 13, 14], it is assumed these values are constant, and we will assume the same here. If not treated as constant, Eq.(21) would be an additional constraint on η^h and $\hat{\mathbf{H}}^h$.

5.4 Stress integration

In order for the plastic dissipation to be defined and stress to remain regular (as opposed to singular), certain conditions on the internal variables and stress result [10, 14]. For the plastic dissipation to be defined, it turns out the inverse of the softening modulus (for strain softening plasticity) must be singular, leading to a regular internal variable [10]. In turn, for the stress $\boldsymbol{\sigma}$ to be regular, its singular part must be zero, which constrains the form of the post-bifurcation, traction-displacement model [13, 14]. In the end, given the enhanced strain field and the reparameterization of the displacement field $\mathbf{u}^h = \tilde{\mathbf{u}}^h + \hat{\mathbf{u}}^h$ in Eq.(15), the enhancement function appears in the stress evolution equation [10], which when integrated leads to

$$\boldsymbol{\sigma}^h = \boldsymbol{\sigma}^{\text{tr}} - \mathbf{c}^e : (\mathbf{m} \otimes \nabla f_S^e) \langle \Delta \zeta \rangle \quad (22)$$

where $\boldsymbol{\sigma}^{\text{tr}}$ is the trial stress, $\langle \bullet \rangle$ is the Macaulay bracket, $\Delta \zeta = \zeta_{n+1} - \zeta_n$, and \mathbf{m} is the direction of the jump displacement

$$\mathbf{m} = \text{sign}(T_t) \cos \psi \mathbf{t} + \sin \psi \mathbf{n} \quad (23)$$

5.5 Implicit integration of traction-displacement model

For implementation by the EDE, the traction-displacement model is integrated using a Backward Euler scheme. For cleaner presentation, variables at the current time step $(\bullet)_{n+1}$ do not have the subscript, whereas those at the past time step $(\bullet)_n$ do. The vector of internal variables \mathbf{q} is integrated as

$$\mathbf{q} = \mathbf{q}_n + \mathbf{h}_q \langle \Delta \zeta \rangle \quad (24)$$

where $\mathbf{h}_q = [h_c h_\phi h_\psi]^T$,

$$\begin{bmatrix} h_c \\ h_\phi \\ h_\psi \end{bmatrix} = \begin{bmatrix} -\alpha_c(c_p - c_r) \exp[-\alpha_c \gamma_\delta] \cos \psi \\ -\alpha_\phi(\phi_p - \phi_r) \exp[-\alpha_\phi \gamma_\delta] \cos \psi \\ -\alpha_\psi \psi_p \exp[-\alpha_\psi \gamma_\delta] \cos \psi \end{bmatrix} \quad (25)$$

and

$$\gamma_\delta = (\gamma_\delta)_n + \cos \psi \langle \Delta \zeta \rangle \quad (26)$$

Note the Macaulay bracket on $\Delta \zeta$. It is possible numerically, especially at the onset of localization (just as bifurcation is detected), that during the iteration process, the value of ζ could oscillate slightly, and $\langle \Delta \zeta \rangle$ ensures that ζ is always positive. Once ζ begins to evolve along the discontinuity surface \mathcal{S} , the oscillations no longer occur. The direction of jump displacement $[\mathbf{u}]$ is handled by the direction \mathbf{m} as defined in Eq.(23), which is a function of the direction of the tangential component of traction on \mathcal{S} , $\text{sign}(T_t)$.

5.6 Galerkin form of traction-displacement model

We can rewrite the yield function in Eq.(13) as

$$F = (\boldsymbol{\mu}^\phi \otimes \mathbf{n}) : \boldsymbol{\sigma} - c = 0 \quad (27)$$

$$\boldsymbol{\mu}^\phi = \text{sign}(T_t) \mathbf{t} + (\tan \phi) \text{sign}(T_n^*) \mathbf{n} \quad (28)$$

where

$$\text{sign}(T_n^*) = \begin{cases} 0 & T_n^* > 0 \text{ tension} \\ 1 & T_n^* < 0 \text{ compression} \end{cases} \quad (29)$$

Applying the method of weighted residuals to Eq.(27), expressing in Galerkin form [15], and dividing by $A_{\mathcal{S}^h}$, we have

$$\frac{1}{A_{\mathcal{S}^h}} \int_{\mathcal{S}^h} \eta^h [(\boldsymbol{\mu}^\phi \otimes \mathbf{n}) : \boldsymbol{\sigma} - c] da = 0 \quad (30)$$

If we choose $\hat{\mathbf{H}}^h = (\boldsymbol{\mu}^\phi \otimes \mathbf{n})$, and we assume η^h is constant over \mathcal{S}^h (which will lead to a constant jump displacement ζ over \mathcal{S}^h [10]), we can write the weak form as

$$\frac{1}{A_{\mathcal{S}^h}} \int_{\mathcal{S}^h} \hat{\mathbf{H}}^h : \boldsymbol{\sigma} da - c = 0 \quad (31)$$

Recall the orthogonality condition Eq.(21) with constant η^h

$$\frac{1}{A_{\mathcal{S}^h}} \int_{\mathcal{S}^h} \hat{\mathbf{H}}^h : \boldsymbol{\sigma}^h da = \frac{1}{V_{\text{loc}}^h} \int_{\Omega_{\text{loc}}^h} \hat{\mathbf{H}}^h : \boldsymbol{\sigma}^h dv \quad (32)$$

which means we can write the weak form as an integration over the volume of the element, allowing us to use the stresses evaluated at the Gauss points to calculate the traction \mathbf{T} along \mathcal{S}^h .

In summary, the complete Galerkin form written in residual form is

$$\begin{aligned} R(\boldsymbol{\sigma}) &= \int_{\Omega^h} \boldsymbol{\nabla} \tilde{\mathbf{w}}^h : \boldsymbol{\sigma}^h dv - \int_{\Omega^h} \tilde{\mathbf{w}}^h \cdot \mathbf{b} dv \\ &\quad - \int_{\Gamma_t^h} \tilde{\mathbf{w}}^h \cdot \mathbf{t}^\sigma da = 0 \end{aligned} \quad (33)$$

$$r(\boldsymbol{\sigma}, \mathbf{q}) = \frac{1}{V_{\text{loc}}^h} \int_{\Omega_{\text{loc}}^h} \hat{\mathbf{H}}^h : \boldsymbol{\sigma} dv - c = 0 \quad (34)$$

We will take advantage of the fact that ζ is discontinuous between elements, a result of the assumed enhanced strain implementation, and condense out Eq.(34) when solving for the compatible displacements at the nodes.

5.7 Yield check along \mathcal{S}^h

We calculate the trial yield value along \mathcal{S}^h by

$$F^{\text{tr}} = \frac{1}{V_{\text{loc}}^h} \int_{\Omega_{\text{loc}}^h} (\hat{\mathbf{H}}^h)^{\text{tr}} : \boldsymbol{\sigma}^{\text{tr}} dv - c_n$$

where

$$\begin{aligned} (\hat{\mathbf{H}}^h)^{\text{tr}} &= (\boldsymbol{\mu}^{\phi_n} \otimes \mathbf{n}) \\ \boldsymbol{\mu}^{\phi_n} &= \text{sign}(T_t^{\text{tr}}) \mathbf{t} + (\tan \phi_n) \text{sign}[(T_n^*)^{\text{tr}}] \mathbf{n} \end{aligned}$$

If $F^{\text{tr}} > 0$ there is yielding along \mathcal{S}^h , and ζ will evolve. Otherwise, the internal variables and ζ will be held fixed.

5.8 Linearization of finite element equations

Let us first write Eq.(33) in finite element matrix form as

$$\begin{aligned} \mathbf{R}(\boldsymbol{\sigma}) &= \int_{\Omega^h} \mathbf{B}^T \cdot \boldsymbol{\sigma}^h dv - \int_{\Omega^h} \mathbf{N}^T \cdot \mathbf{b} dv \\ &\quad - \int_{\Gamma_t^h} \mathbf{N}^T \cdot \mathbf{t}^\sigma da = 0 \end{aligned} \quad (35)$$

where \mathbf{B} is the strain-displacement matrix, and \mathbf{N} is the vector of nodal shape functions. When linearizing the residuals in Eqs.(35,34) about an iteration state k , we have (leaving off $k + 1$ for current iteration)

$$\delta \mathbf{R}(\boldsymbol{\sigma}) = \frac{\partial \mathbf{R}}{\partial \boldsymbol{\sigma}} \cdot \delta \boldsymbol{\sigma} = -\mathbf{R}^k \quad (36)$$

$$\delta r(\boldsymbol{\sigma}, \mathbf{q}) = \frac{\partial r}{\partial \boldsymbol{\sigma}} \cdot \delta \boldsymbol{\sigma} + \frac{\partial r}{\partial \mathbf{q}} \cdot \delta \mathbf{q} = -r^k \quad (37)$$

where $\delta(\bullet) = (\bullet)^{k+1} - (\bullet)^k$ and

$$\delta \boldsymbol{\sigma} = \frac{\partial \boldsymbol{\sigma}}{\partial \mathbf{d}} \cdot \delta \mathbf{d} + \frac{\partial \boldsymbol{\sigma}}{\partial \mathbf{q}} \cdot \delta \mathbf{q} + \frac{\partial \boldsymbol{\sigma}}{\partial \zeta} \delta \zeta \quad (38)$$

$$\delta \mathbf{q} = \frac{\partial \mathbf{h}_q}{\partial \mathbf{q}} \cdot \delta \mathbf{q} \langle \Delta \zeta \rangle + \frac{\partial \mathbf{q}}{\partial \zeta} \delta \zeta \quad (39)$$

where \mathbf{d} is the vector of nodal displacements. When rearranging Eq.(39), we find

$$\delta \mathbf{q} = \frac{\widehat{\partial \mathbf{q}}}{\partial \zeta} \delta \zeta \quad (40)$$

$$\begin{aligned} \frac{\widehat{\partial \mathbf{q}}}{\partial \zeta} &:= \left(\mathbf{1} - \langle \Delta \zeta \rangle \frac{\partial \mathbf{h}_q}{\partial \mathbf{q}} \right)^{-1} \\ &\quad \times \left(\frac{\partial \mathbf{h}_q}{\partial \zeta} \langle \Delta \zeta \rangle + \mathbf{h}_q \langle \text{sign}(\Delta \zeta) \rangle \right) \end{aligned} \quad (41)$$

Skipping some steps, we end up with

$$\begin{aligned} \frac{\partial \mathbf{R}}{\partial \mathbf{d}} \cdot \delta \mathbf{d} + \frac{\partial \mathbf{R}}{\partial \zeta} \delta \zeta &= -\mathbf{R}^k \\ \frac{\partial r}{\partial \mathbf{d}} \cdot \delta \mathbf{d} + \frac{\partial r}{\partial \zeta} \delta \zeta &= -r^k \end{aligned} \quad (42)$$

where

$$\begin{aligned} \frac{\partial \mathbf{R}}{\partial \mathbf{d}} &= \int_{\Omega^h} \mathbf{B}^T \cdot \mathbf{D}^e \cdot \mathbf{B} dv \\ \frac{\partial \mathbf{R}}{\partial \zeta} &= \int_{\Omega^h} \mathbf{B}^T \cdot \frac{\partial \boldsymbol{\sigma}}{\partial \zeta} dv \\ \frac{\partial r}{\partial \mathbf{d}} &= \frac{1}{V_{\text{loc}}^h} \int_{\Omega_{\text{loc}}^h} (\boldsymbol{\mu}^\phi \otimes \mathbf{n}) \cdot \mathbf{D}^e \cdot \mathbf{B} dv \\ \frac{\partial r}{\partial \zeta} &= \frac{1}{V_{\text{loc}}^h} \int_{\Omega_{\text{loc}}^h} (\boldsymbol{\mu}^\phi \otimes \mathbf{n}) : \frac{\partial \boldsymbol{\sigma}}{\partial \zeta} dv + \frac{\partial r}{\partial \mathbf{q}} \cdot \frac{\widehat{\partial \mathbf{q}}}{\partial \zeta} \end{aligned}$$

and \mathbf{D}^e is the matrix form of the elastic modulus tensor \mathbf{c}^e . Furthermore, we can write Eq.(42) as

$$\begin{aligned} \mathbf{K}_{dd} \cdot \delta \mathbf{d} + \mathbf{K}_{d\zeta} \delta \zeta &= -\mathbf{R}^k \\ \mathbf{K}_{\zeta d} \cdot \delta \mathbf{d} + K_{\zeta\zeta} \delta \zeta &= -r^k \end{aligned}$$

and when statically condensing out $\delta \zeta$, we have the following equation to solve for $\delta \mathbf{d}$

$$\begin{aligned} (\mathbf{K}_{dd} - K_{\zeta\zeta}^{-1} \mathbf{K}_{d\zeta} \otimes \mathbf{K}_{\zeta d}) \cdot \delta \mathbf{d} &= \\ -\mathbf{R}^k + (r^k / K_{\zeta\zeta}) \mathbf{K}_{d\zeta} \end{aligned} \quad (43)$$

With $\delta \mathbf{d}$ solved from Eq.(43), we can solve for $\delta \zeta$

$$\delta \zeta = -(r^k + \mathbf{K}_{\zeta d} \cdot \delta \mathbf{d}) / K_{\zeta\zeta} \quad (44)$$

Using this linearization, we then iterate until we reach convergence $\|\mathbf{R}^{k+1}\| / \|\mathbf{R}^0\| < \text{tol}_R$ and $|r^{k+1}| / |r^0| < \text{tol}_r$.

5.9 Linear softening traction-displacement model

The discussion up to this point has been based on an exponential softening traction-displacement model. Here, we present equations for a linear softening model. The vector of internal variables \mathbf{q} is integrated as

$$\mathbf{q} = \mathbf{q}_n + \mathbf{h}_q \langle \Delta \zeta \rangle \quad (45)$$

where

$$\mathbf{h}_q = \begin{bmatrix} h_c \\ h_\phi \\ h_\psi \end{bmatrix} = \begin{bmatrix} -\alpha_c \cos \psi \\ -\alpha_\phi \cos \psi \\ -\alpha_\psi \cos \psi \end{bmatrix} \quad (46)$$

and

$$\gamma_\delta = (\gamma_\delta)_n + \cos \psi \langle \Delta \zeta \rangle \quad (47)$$

Numerical examples will present the use of both exponential and linear softening models.

5.10 Continuous stress in time at bifurcation point

In order to ensure that the stress is continuous in time at the point of bifurcation, the peak cohesion c_p is calculated from Eq.(34) within an element e as

$$c_p = \frac{1}{V_{\text{loc}}^e} \int_{\Omega_{\text{loc}}^e} \hat{\mathbf{H}}^e : \boldsymbol{\sigma}_n dv \quad (48)$$

where V_{loc}^e is the localized element volume, Ω_{loc}^e its domain, $\hat{\mathbf{H}}^e$ its enhancement function multiplier, and $\boldsymbol{\sigma}_n$ the converged stress from the past time step t_n before bifurcation was detected in the element e .

6. NUMERICAL EXAMPLES

3D plane strain and corner shear examples demonstrate the aforementioned models and EDE implementation.

6.1 Plane strain compression

To verify that the post-bifurcation model is working (although there is no analytical solution to conduct a true verification), we consider a plane strain compression problem for rate-insensitivity $\tau = 0$. Parameters in Table 1 are used for the bulk material (Salem Limestone). Parameters for the exponential post-bifurcation traction-displacement model are given in Table 2, and for the linear traction-displacement model in Table 3.

| Symbol | Value |
|---------------|------------|
| c_p | calculated |
| c_r | 10 MPa |
| ϕ_p | 0.5236 rad |
| ϕ_r | 0.1 rad |
| ψ_p | 0.087 rad |
| α_c | 1e3 1/m |
| α_ϕ | 9e2 1/m |
| α_ψ | 9e2 1/m |

Table 2. Parameters for plane strain compression: post-bifurcation, exponential softening model. Note that the peak cohesion c_p is calculated from Eq.(48) in order to ensure that the stress is continuous in time at bifurcation.

Figure 7 demonstrates the post-bifurcation exponential softening for the EDE. The darker shaded top face of the element is displaced downward in the $-x_2$ direction, the lighter shaded faces are traction free, and the clear faces are fixed in displacement normal to the face. Since there is no asymmetry or inhomogeneity to determine which \mathbf{n} to choose as the normal to the discontinuity surface \mathcal{S} , we choose the negative angle $-\theta$.

Figure 8 shows the deformed element looking perpendicular to the x - y plane. The left figure shows the compatible displacement $\tilde{\mathbf{u}}^h$ for the deformed element, while the right figure shows the total displacement \mathbf{u}^h , reconstructed given ζ . Note that for the right figure, the nodal displacements are the compatible displacement $\tilde{\mathbf{u}}^h$. The solid circles are the deformed element nodes, while the open circles are the

undeformed element nodes. The dashed line shows the undeformed element, while the solid line shows the deformed element. Note that when viewing the deformed mesh, the left figure would be observed, which accounts for the jump displacement, while the right figure was reconstructed given ζ .

Figures 9 and 10 show the cohesion, friction, and dilation exponential softening, respectively.

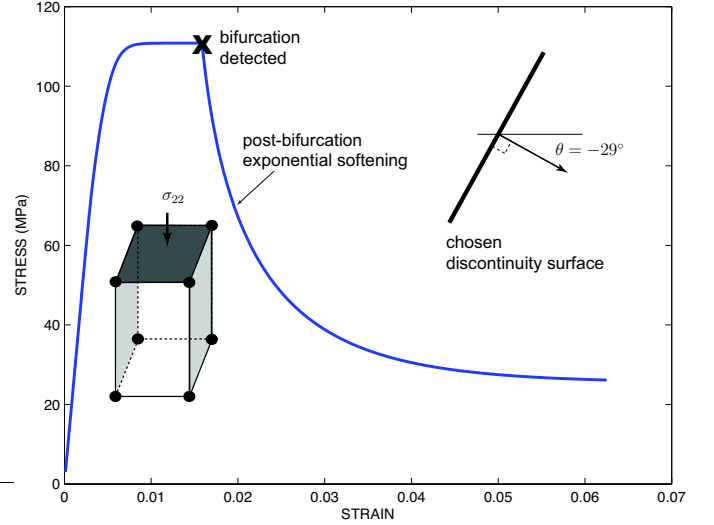


Figure 7. Plot of stress versus strain for bifurcation and post-bifurcation analysis (exponential softening) of plane strain compression of Salem Limestone using the Sandia GeoModel.

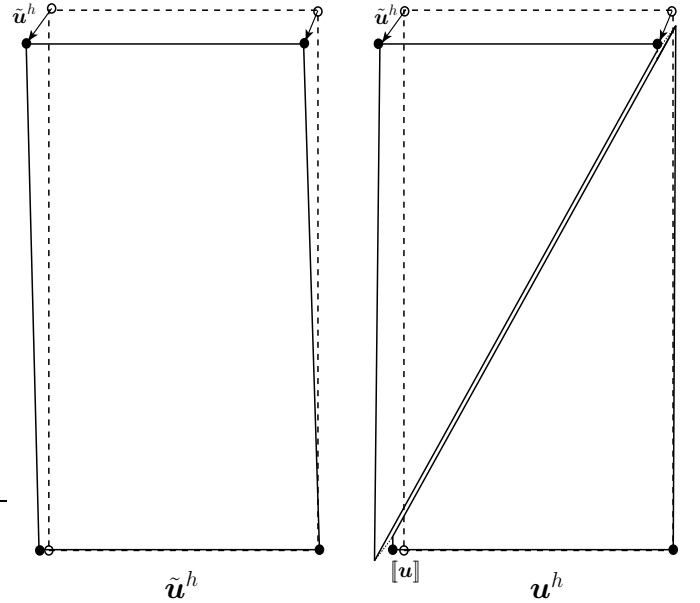


Figure 8. Deformed element at end of deformation in Fig.7 ($\approx 6\%$ strain, $\zeta \approx 4.5\text{mm}$).

Figure 11 demonstrates the post-bifurcation linear softening for the embedded discontinuity element. Note the asymptotic behavior to a residual value.

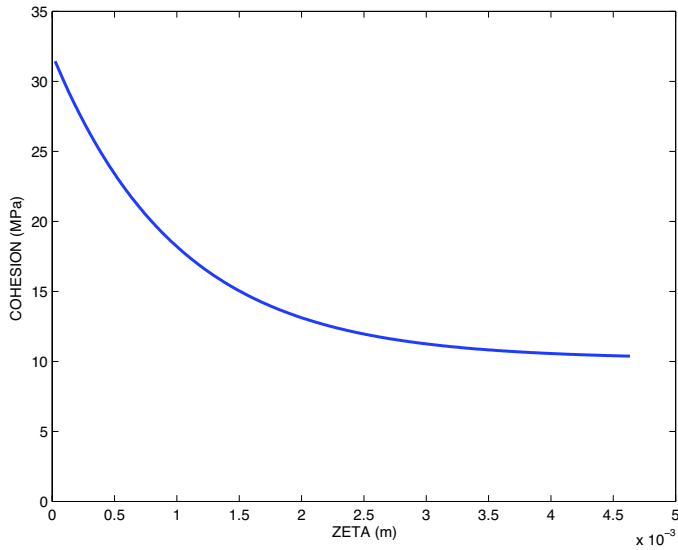


Figure 9. Plot of cohesion c versus jump displacement magnitude ζ for bifurcation and post-bifurcation analysis (exponential softening) of plane strain compression of Salem Limestone using the Sandia GeoModel. Note the asymptotic behavior to the residual value $c_r = 10$ MPa.

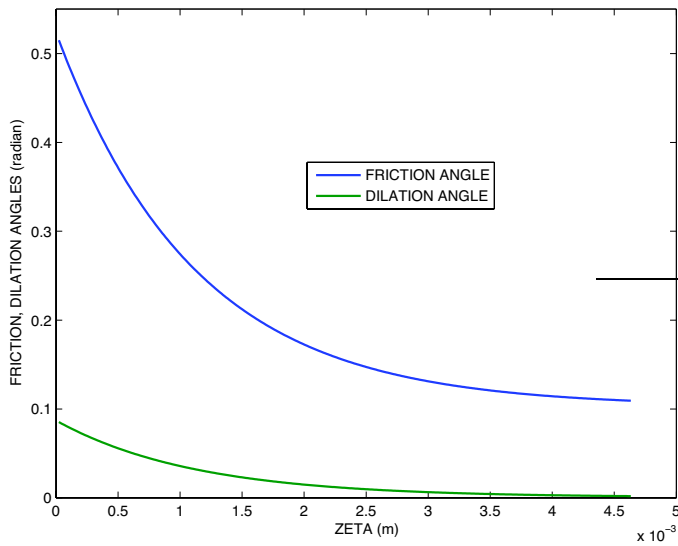


Figure 10. Plot of friction angle ϕ and dilation angle ψ versus jump displacement magnitude ζ for bifurcation and post-bifurcation analysis (exponential softening) of plane strain compression of Salem Limestone using the Sandia GeoModel. Note the asymptotic behavior to the residual values $\phi_r = 0.1$ and $\psi_r = 0$ radians.

There are two post-bifurcation slopes. The first is a result of the combined cohesion, friction, and dilation softening, and the second is a result of only friction softening as the cohesion and dilation have reached their residual values (cf. Figs. 12 and 13).

Figures 12 and 13 show the cohesion, friction, and dilation linear softening, respectively.

| Symbol | Value |
|---------------|------------|
| c_p | calculated |
| c_r | 10 MPa |
| ϕ_p | 0.5236 rad |
| ϕ_r | 0.1 rad |
| ψ_p | 0.087 rad |
| α_c | 1e4 MPa/m |
| α_ϕ | 1e2 rad/m |
| α_ψ | 1e2 rad/m |

Table 3. Parameters for plane strain compression: post-bifurcation, linear softening model.

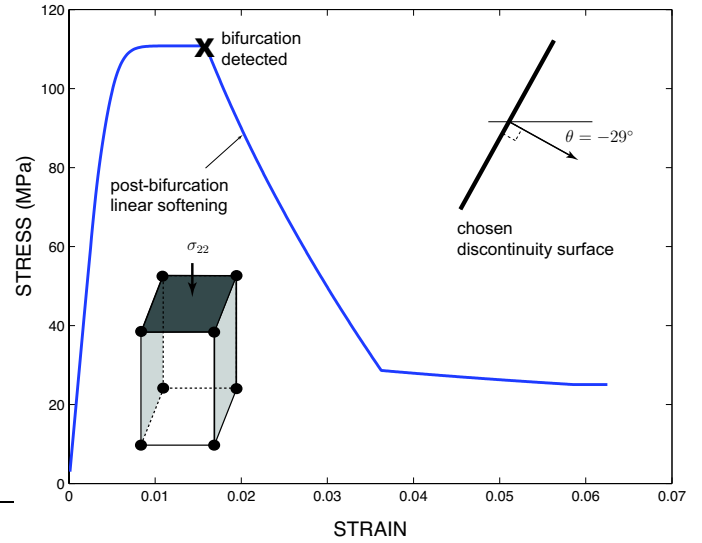


Figure 11. Plot of stress versus strain for bifurcation and post-bifurcation analysis (linear softening) of plane strain compression of Salem Limestone using the Sandia GeoModel.

6.2 3D corner shear

For testing the true three-dimensional nature of the EDE, we consider a corner shear problem using eight trilinear hexahedral elements. Post-bifurcation, linear softening parameters are given in Table 4. A Drucker-Prager strain-softening plasticity model was used in place of the Sandia GeoModel because for this particular example the Sandia GeoModel and its parameters could not predict bifurcation.

Figure 14 demonstrates the post-bifurcation softening for corner shear loading. In this case, only the corner node enhancement function is activated, as indicated in Fig.6. This demonstrates a problem that cannot be solved using a 2D plane strain formulation [12, 13, 14].

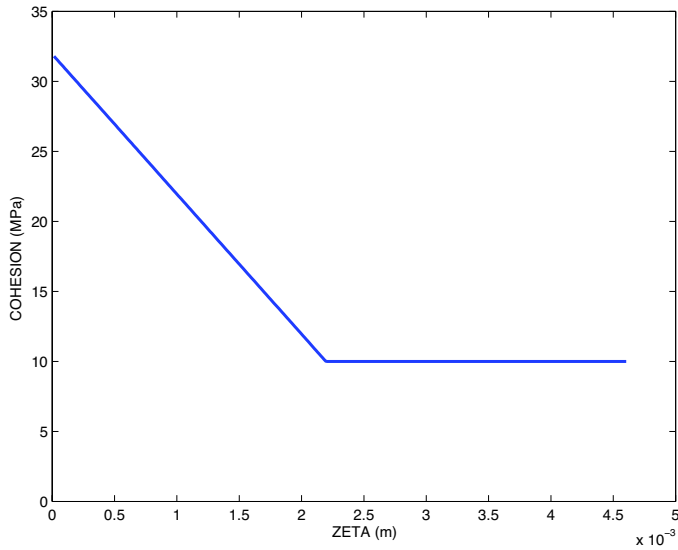


Figure 12. Plot of cohesion c versus jump displacement magnitude ζ for bifurcation and post-bifurcation analysis (linear softening) of plane strain compression of Salem Limestone using the Sandia GeoModel. Note the cut-off at the residual value $c_r = 10$ MPa.

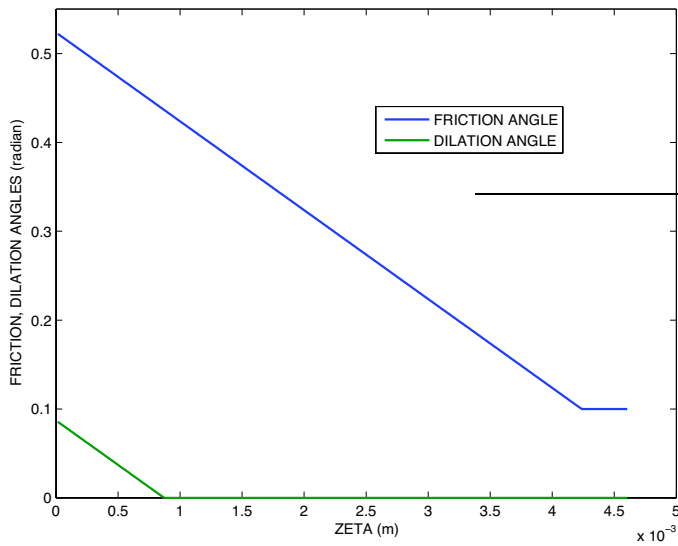


Figure 13. Plot of friction angle ϕ and dilation angle ψ versus jump displacement magnitude ζ for bifurcation and post-bifurcation analysis (linear softening) of plane strain compression of Salem Limestone using the Sandia GeoModel. Note the cut-off at the residual values $\phi_r = 0.1$ and $\psi_r = 0$ radians.

7. CONCLUSIONS

The paper presented a 3D Embedded Discontinuity finite Element (EDE) formulation and implementation, and demonstrated it using a simple Mohr-Coulomb failure model with exponential and linear softening. A corner shear example demonstrated the true three-dimensionality of the new element. Further work will present more complex boundary value

| Symbol | Value |
|---------------|------------|
| c_p | calculated |
| c_r | 0 MPa |
| ϕ_p | 0.5236 rad |
| ϕ_r | 0.0 rad |
| ψ_p | 0.1 rad |
| α_c | 3e8 MPa/m |
| α_ϕ | 1e3 rad/m |
| α_ψ | 1e3 rad/m |

Table 4. Parameters for 3D corner shear: post-bifurcation, linear softening model.

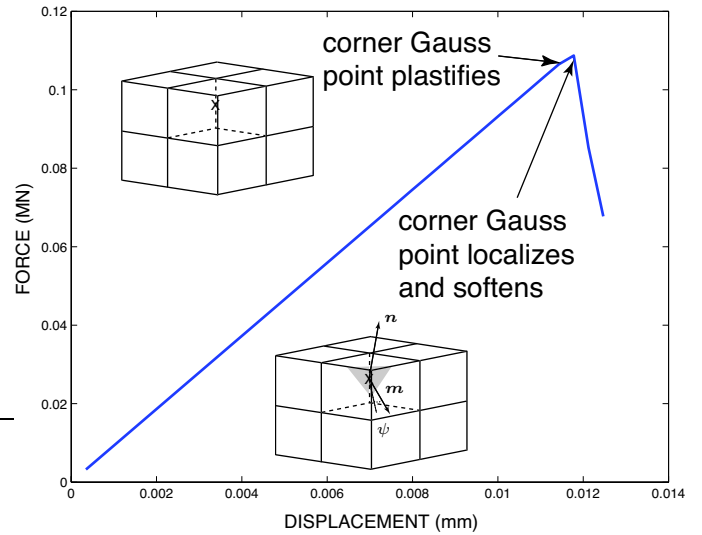


Figure 14. Post-peak softening in corner element of eight trilinear hexahedral element mesh for corner shear.

problems of interest to geological engineering.

8. ACKNOWLEDGEMENTS

The author acknowledges C.D. Foster for implementing the numerical algorithm in Tahoe (tahoe.ca.sandia.gov) for detecting loss of ellipticity of the acoustic tensor for 3D stress states, and for implementing the Sandia GeoModel in Tahoe as discussed in [3].

REFERENCES

- [1] Regueiro, R.A., Foster, C.D., Fossum, A.F., Borja, R.I. 2004 Bifurcation analysis of a three-invariant, isotropic/kinematic hardening cap plasticity model for geomaterials, ARMA/NARMS 04-520.
- [2] A. F. Fossum, A.F., and R. M. Brannon. 2004. *The Sandia GeoModel: Theory and User's Guide*. Sandia National Laboratories. SAND2004-3226.
- [3] Foster, C.D., R.A. Regueiro, A.F. Fossum, and R.I. Borja. 2005. Implicit integration of a three-invariant, single-surface, isotropic/kinematic hardening, cap plasticity model for geomaterials. *Comput. Methods Appl. Mech. Engrg.* 194:5109–5138.
- [4] Sandler, I.S. and J.P. Wright. 1984. Strain-softening. In *Theoretical Foundations for Large Scale Computations of Nonlinear Material Behavior*, eds. S. Nemat-Nasser et al., 285–315, Martinus Nijhoff Pub., The Netherlands.
- [5] Needleman, A. 1988. Material rate dependence and mesh sensitivity in localization problems. *Comput. Methods Appl. Mech. Engrg.* 67: 69–85.
- [6] Sluys, L.J. and R. de Borst. 1992. Wave propagation and localization in a rate-dependent cracked medium: Model formulation and one-dimensional examples. *Int. J. Solids Struct.* 29: 2945–2958.
- [7] Rice, J.R. and J.W. Rudnicki. 1980. A note on some features of the theory of localization of deformation. *Int. J. Solids Struct.* 16: 597–605.
- [8] Simo, J.C., and M.S. Rifai. 1990. A class of mixed assumed strain methods and the method of incompatible modes. *Int. J. Numer. Methods Eng.* 29:1595–1638.
- [9] Simo, J.C., and A. Armero. 1992. Geometrically nonlinear enhanced strain mixed methods and the method of incompatible modes. *Int. J. Numer. Methods Eng.* 33:1413–49.
- [10] Simo, J.C., J. Oliver, and F. Armero. 1993. An analysis of strong discontinuities induced by strain-softening in rate-independent inelastic solids. *Comput. Mech.* 12: 277–296.
- [11] Armero, F., and K. Garikipati. 1996. An analysis of strong discontinuities in multiplicative finite strain plasticity and their relations with the numerical simulation of strain localization in solids. *Int. J. Solids Struct.* 33:2863–85.
- [12] Regueiro, R.A., and R.I. Borja. 1999. Finite element model of localized deformation in frictional materials taking a strong discontinuity approach. *Finite Elem. Anal. Des.* 33:283–315.
- [13] Borja, R.I., and R.A. Regueiro. 2001. Strain localization in frictional materials exhibiting displacement jumps. *Comput. Methods Appl. Mech. Engrg.* 190:2555–80.
- [14] Regueiro, R.A., and R. I. Borja. 2001. Plane strain finite element analysis of pressure sensitive plasticity with strong discontinuity. *Int. J. Solids Struct.* 38:3647–72.
- [15] T. J. R. Hughes. 1987. *The Finite Element Method*. Prentice-Hall: New Jersey.
- [16] Taylor, R.L., J.C. Simo, O.C. Zienkiewicz, and A.C.H. Chan. 1986. Patch test - A condition for assessing FEM convergence. *Int. J. Numer. Methods Eng.* 22:39–62.